19

High-Bias Instability of Atomic and Molecular Junctions

Akira Sakai
Kyoto University
Japan

1. Introduction

Atom-sized contacts are appealing interconnects in atomic- and molecular-scale devices. Because these contacts are smaller than the mean free path of electrons, conduction electrons are rarely scattered when they pass through the contact. This absence of scattering events not only ensures high electron mobility but also achieves small energy dissipation at the contact. As a result, we can obtain in atom-sized contacts a huge current density that is unattainable for present-day microfabricated interconnects. A single-atom contact of Au, for example, is capable of sustaining a current density as high as 8×10^{10}A/cm^2 (Yanson et al., 1998), which is orders of magnitude higher than the current density realized in microelectronics devices. However, atom-sized contacts would eventually become unstable and break down when they are subject to sufficiently high biases or high currents. This stability limit of atom-sized contacts is of much value both in application and in academia. In electronics applications, the magnitude of allowable bias or current is a critical parameter because it directly determines the maximum rating of atom-sized contacts when they are incorporated into real devices. For atom-sized contacts, even a low voltage such as 3 V, commonly used in CMOS devices, can be regarded as a high bias which, in the case of an Au single-atom contact, would generate a current density that well exceeds the maximum value mentioned above. On the other hand, typical molecular FETs would operate under biases much higher than 3 V and hence achieve current densities far exceeding the maximum value. It is therefore practically quite important to know the stability limit of the atom-sized contacts under high-bias/current conditions.

The same stability problem also provides us a fertile ground of physical investigations. The high-bias/current instability of atom-sized contacts involves various microscopic processes which have not yet been fully worked out. When one applies a high bias to an atom-sized contact, hot electrons are injected from one electrode into the contact. Though the contact is smaller in size than the electronic mean free path, there still remains a non-zero chance for the hot electrons to interact with the lattice and partly transfer their kinetic energy, and/or momentum, to the contact atoms, often causing their vibrational heating and electromigration. At the downstream electrode, electrons dissipate their energy which diffuses out to the bulk through the lattice heat conduction. All these processes are individually well studied in macroscopic materials but little understood for ultrasmall conductors such as the atom-sized contacts. To obtain some insight on this topic of practical and academic interest, some

theories are currently emerging on the high-bias/current instability of atom-sized contacts, and systematic measurements are now called for to provide a solid database for further theoretical and experimental developments.

2. Contact lifetime

At the present time, microscopic theories have been proposed for specific high-bias problems, and there has been no general theoretical framework that can be universally used for analyzing various experimental data. A crude way for dealing with the stability problem is to consider the contact lifetime τ and employ the following empirical formula, (Smit et al., 2004)

$$\tau = \tau_0 \exp\left(\frac{E(V,F)}{k_B T^*}\right), \tag{1}$$

where T^* is an effective contact temperature and $E(V,F)$ is a stabilization energy of the contact at a bias voltage V and under a tensile force F. The latter is included in the stabilization energy because the atom-sized contacts are often produced by pulling apart macroscopic metal-metal contacts, as will be mentioned in the next section. Atom-sized contacts formed by such junction breaking always involve some internal tension, the strength of which is not negligible.
Within a linear approximation, $E(V,F)$ can be written as,

$$E(V,F) = E_0 - \alpha V - \beta F \tag{2}$$

where E_0 is the stabilization energy at $V = 0$ and $F = 0$, and the coefficients α and β represent the bias and the tensile-force sensitivity of E, respectively. Then we obtain,

$$\tau = \tau_0 \exp\left(\frac{E_0 - \alpha V - \beta F}{k_B T^*}\right). \tag{3}$$

This equation is purely empirical and has no rigorous theoretical basis for it. However, similar thermal-activation type formula has been widely used for describing the rate of atomic jumps during electromigration in nanocontacts, and Eq. 3 would thus be a reasonable first approximation for the lifetime of atom-sized contacts under high biases. According to Eq. 3, either V or F reduces E and tends to destabilize the contact. If one increases V while keeping F constant, E becomes comparable to thermal energy at $V_b = (E_0 - \beta F - k_B T^*)/\alpha$. This bias determines the break voltage of the contact. On the other hand, if one increases F at zero or low constant biases, the contact becomes unstable at $F_b = (E_0 - \alpha V - k_B T^*)/\beta$, which defines the maximum tensile strength of the contact.
Under high bias/current conditions, Joule heating of contacts is indeed non-negligible, and this is the reason why the effective temperature T^*, not the ambient temperature T, enters in Eqs. 1 and 3. In the case of atom-sized contacts, the contact overheating mainly depends on how fast the generated heat is carried away by the lattice thermal transport. Todorov and coworkers (Todorov et al., 2001) theoretically studied this heat generation/diffusion problem and proposed the following formula for T^*,

$$T^{*4} = T^4 + \gamma(LV)^2 = T^4 + T_V^4, \qquad T_V \equiv \gamma^{1/4}\sqrt{LV} \tag{4}$$

where L is a contact length and γ is a material-dependent constant which takes $\gamma \sim 60$ $\mathrm{KV}^{-1/2}\mathrm{nm}^{-1/2}$ for typical metals (Todorov et al., 2001). Because the contribution of the ambient temperature in Eq. 4 increases as T^4, the bias-dependent second term is negligible compared to the first term at room temperature, and hence we have $T^* \sim T$. On the contrary, the second term becomes dominant at liquid helium temperature where T^* increases with the bias as $T^* \propto \sqrt{LV}$ (**?**).

The magnitude of T^* can be evaluated experimentally by measuring the frequency of the conductance two-level fluctuations (TLFs) often observed on the atom-sized contacts. This stochastic switching of the conductance is caused by the thermally activated jumps of an atom locating near the constriction, and the TLF frequency varies with the contact temperature. Tsutsui *et al.* (Tsutsui et al., 2006a) measured the TLF frequency of Au atom-sized contacts at 4 K under different biases and showed that their TLF data consistently fit to the $\sqrt{V}$ dependence of T^*. According to their results, a contact at $T = 4$ K under a bias of 1.0 V becomes heated up to $T^* \sim 75$ K.

Compared to T^*, little has been known on the stabilization energy E_0 and the coefficients α and β in Eq. 3. Tsutsui *et al.* (Tsutsui et al., 2006b) analyzed the bias dependence of the conductance TLF frequency of noble metal contacts and obtained nearly the same value $\alpha \sim 0.1$ eV/V for Au, Ag and Cu. Smit *et al.* (Smit et al., 2004) showed that their break voltage data on the single-atom contacts of Au and Pt can be consistently described by Eqs. 3 and 4. From the data fitting, they estimated $E_0 = 0.738$ eV, $\alpha = 0.14$ eV/V and $\beta = 0.49$ eV/nN for Au. On the other hand, Tsutsui *et al.* (Tsutsui et al., 2008) directly measured τ of the Au single-atom contacts at room temperature. By fitting the observed data with Eq. 3, they obtained $\beta \sim 0.1$ eV/nN. For metals other than Au, no experimental data are available at this time on β and E_0.

3. Conductance of atom-sized contacts of metals

Atom-sized contacts of metals are too small to be observed by conventional tools so that, except for some studies using high-resolution transmission-electron microcopy, we have no direct means to tell whether these ultrasmall contacts are actually formed or not. Instead of direct observations, therefore, we usually measure the junction conductance G and use its magnitude as a convenient measure of the junction size. In the case of macroscopic conductors larger than the mean free path of electrons, a conductance G of a constriction can be expressed as $G \propto 1/d$ (Agraït et al., 2003) where d is the constriction diameter. When d becomes smaller than the mean free path, the flow of free electrons through such a small constriction is physically analogous to the gas flow through a small orifice, and the gas conductance formula for a circular orifice of diameter d in the molecular flow regime can be transformed into that for the electronic conductance. This leads to the following conductance formula (Agraït et al., 2003),

$$G = \frac{2e^2}{16h}(k_F d)^2 = \frac{2e^2}{4\pi h}k_F^2 A, \tag{5}$$

where is k_F the electron Fermi wavelength and $A = \pi d^2/4$ is the contact cross-sectional area. This is the Sharvin conductance formula which applies for conductors smaller than the electronic mean free path.

When d becomes even smaller and comparable to the Fermi wavelength, the contact electrons can no longer be regarded as free electrons but as valence electrons of contact atoms. In

this atomistic limit, the contact conductance is determined, roughly speaking, by how freely electrons can pass through the valence electronic states of the contact. If a contact has n valance states, its conductance can be written as,

$$G = \frac{2e^2}{h} \sum_n T_n = G_0 \sum_n T_n, \tag{6}$$

where T_n is the electron transmission probability of the n-th state, and $G_0 \equiv 2e^2/h$ is the conductance quantum unit. More precisely, the conductance is determined by the transmission probability of the conductance channels which are a set of orthonormal states constituted from the valence states. This formula is usually referred to as the Landauer conductance formula. When $T_n = 1$ for all states, $G = n(2e^2/h)$ and the conductance becomes quantized in integer multiples of the conductance quantum.

In the quantum point contacts of two-dimensional electron gas, all electronic states are highly transparent, i.e. $T_n = 1$, and the number n of the contact states can be finely controlled by continuously varying the constriction width with a gate voltage. As a result, quantized steps in G in unit of G_0 can be clearly observed. On the other hand, metal contacts cannot be continuously reduced in size because of the atomic discreteness of their lattices. The contact necking often proceeds discontinuously by repeating an elastic stretching followed by an abrupt relaxation or rearrangement of atomic configuration. Reflecting this discrete nature of the necking deformation, the conductance of a nanocontact often exhibits plateaus and steps when it is stretched by applying a tensile force. These stepwise changes in the conductance, however, have no relationship with the variation of the number n of transmission states in Eq. 6 and hence do not represent the quantized changes in conductance, except for some rare cases where the discrete reduction of the contact geometry precisely correlates to that of n. In most contacts, the conductance plateaus correspond to a formation of certain contact geometries that are more stable than others. Such stable contacts make a prolonged elastic deformation under a stretching force and often produce a long conductance plateau. Single-atom contacts of metals are the most stable contact because its failure involves the direct bond breaking. Consequently, single-atom contacts usually display a clear conductance plateau, the last plateau before the contact failure, and we can determine the single-atom conductance from the position of such a last conductance plateau. Also, we can know the formation of a single-atom contact by detecting this conductance plateau.

The electron transmission probability T_n in Eq. 6 varies with the valence characteristics of the state n. A general trend is that all s states and some sp states that extend along the contact axis show a high transmission, i.e. $T_n \sim 1$, while localized d states transmit electrons only partially (Cuevas et al., 1998). Monovalent noble metals such as Au, Ag, and Cu has one s-like valence state. As a result, the single-atom contact of these noble metals has a single conductance channel which shows $T_n \sim 1$ and hence $G \sim 1G_0$ according to Eq. 6. Experimentally, noble-metal contacts are known to exhibit a clear conductance plateau at $1G_0$ when they are reduced to the size of atoms. The experimental results are thus in good agreement with Eq. 6, and it is now well established that the single-atom conductance of noble metals is $1G_0$. This does not necessarily guarantee that the $1G_0$ contacts of noble metals are always a single-atom contact because larger contacts consisting two or more atoms may happen to show the $1G_0$ conductance. However, such conductance coincidence scarcely

occurs, and one can usually identify the $1G_0$ contacts of Au, Ag, and Cu as a single-atom contact.

4. Fabrication method of atom-sized contacts

The break junction method is the most convenient and widely used one for producing atom-sized contacts of metals. This method utilizes the necking deformation of a metal contact to obtain atom-sized contacts. First, a macroscopic contact is formed between a pair of metal electrodes. Then, the electrodes are separated apart to stretch the contact, as schematically illustrated in Fig. 1.

Fig. 1. Formation of an atom-sized contact by breaking a macroscopic contact.

The contact undergoes the necking deformation, shrinks in size, and becomes an atom-sized contact before it completely breaks up. As mentioned in the previous section, the conductance often exhibits plateaus in the course of necking deformation. Figure 2 represents a typical example of the temporal change in the conductance recorded during a breakup of an Au contact at 0.6 V. The last plateau appears at $1G_0$, and this $1G_0$ plateau corresponds to the Au single-atom contact which has the $1G_0$ conductance as explained in the previous section.

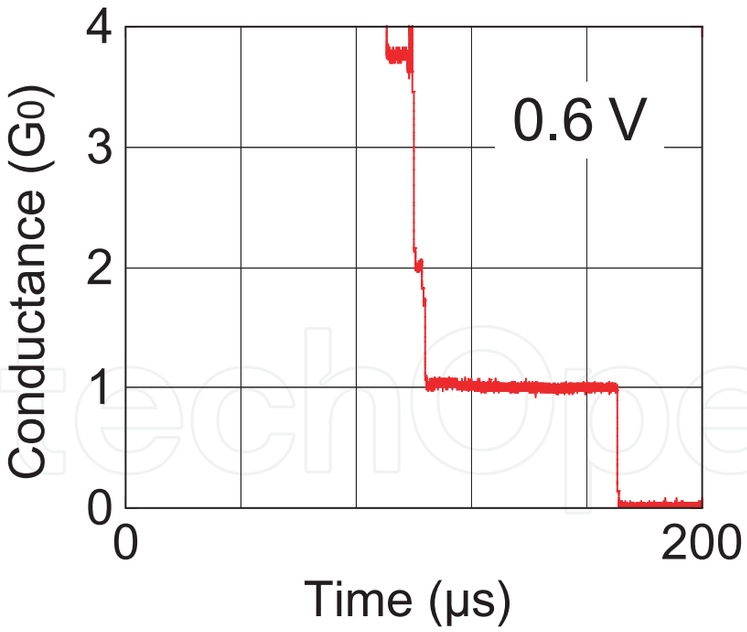

Fig. 2. Temporal change in the conductance of an Au contact during its breakup.

In the break junction method, the geometry of the electrodes and their initial macroscopic contact is irrelevant for the formation of atom-sized contacts, and a wide variety of macroscopic electrodes have been used so far in the past experiments. Figures 3 and 4 display two examples used for studying the high-bias instability of atom-sized contacts.

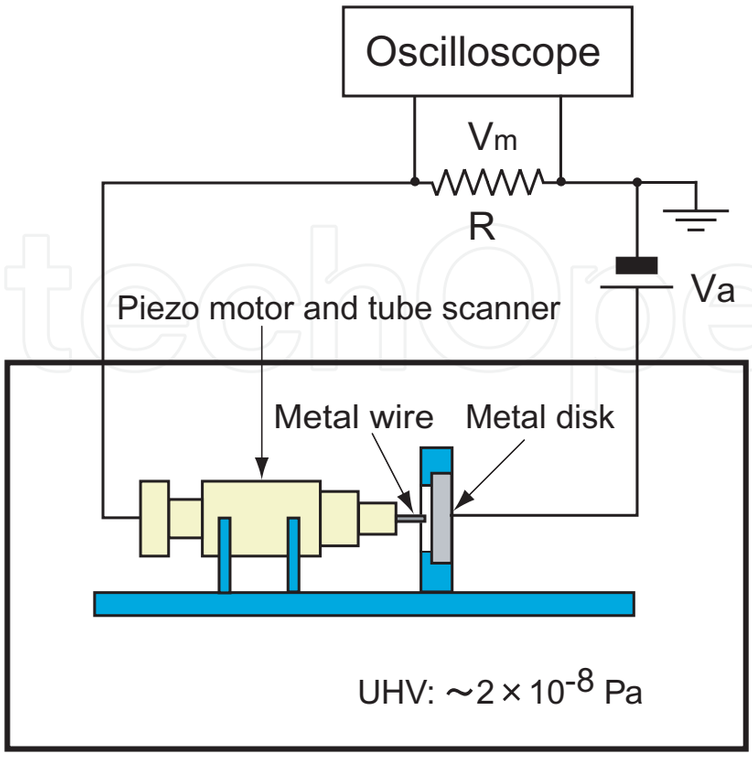

Fig. 3. An apparatus for fabricating wire-disk-type break junctions.

In a setup shown in Fig. 3, a metal wire and a metal disk serve as electrodes. A contact is made and broken by pressing and retracting the wire against the disk. A piezo tube scanner combined with a piezo motor is used for moving the wire and finely controlling its displacement. In Fig. 3, the contact conductance is measured by detecting the voltage drop V_m across a current-sensing resistor R connected in series with the contact. The conductance G is related to V_m though the following equation,

$$G = \frac{V_m}{R(V_a - V_m)}, \tag{7}$$

where V_a is an applied bias. In this measuring setup, the conductance nonlinearly depends on the measured voltage V_m, and the conductance resolution decreases at higher conductances. However, the use of an oscilloscope enables us to record fast transient behaviors of the conductance at and near the onset of instability. Some examples of such transient conductance traces will be shown in Sec. 5.1.

Figure 4 depicts the schematic of MCBJ (mechanically controllable break junction), which is another widely used method for fabricating atom-sized contacts. In the MCBJ, a thin-metal wire is glued at two points onto a flexible substrate. By bending the substrate by a piezo actuator, the wire is broken in the middle between the two fixed points, and each end of the broken wire serves as an electrode. The gap between the electrodes can be made open and closed by extending and retracting the actuator, respectively. Because the reduction ratio between the actuator displacement and the change in the gap distance can be made very large, the gap distance can be finely controlled by the actuator with a resolution of a few

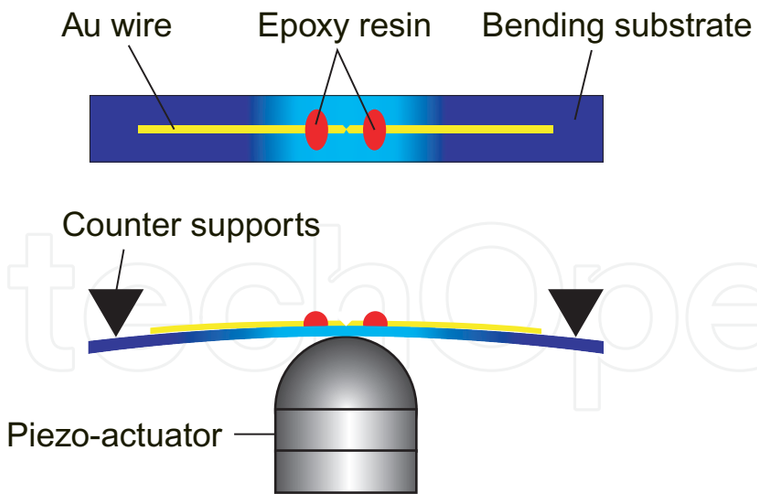

Fig. 4. Schematic of MCBJ (mechanically controllable break junction).

pm. This superior gap controllability of MCBJ, together with its high mechanical stability against disturbances from outside, makes MCBJ a superior method for fabricating atom-sized contacts and nanogapped electrodes for molecules.

5. Experiments on the high-bias /current instability of atom-sized contacts

Two experimental methods have been exploited for studying the high-bias instability of atom-sized contacts. In one method depicted in Fig. 5(a), a macroscopic contact is first prepared and placed under a constant bias voltage. Then, the contact is mechanically stretched to break it. As mentioned in the previous section, this contact stretching makes a necking deformation of the contact and often yields an atom-sized contact before the contact completely breaks up. As the contact necking proceeds, the contact cross section decreases and the current density increases accordingly. At some point during the deformation, the contact becomes unstable against its high current density and ruptures before it makes a mechanical fracture. By observing the threshold for such a contact failure, we can obtain information on the current-induced instability of atom-sized contacts. We will show in the next section experimental results on some metal contacts and explain how we can analyze the data to determine j_c, the threshold current density for the instability.

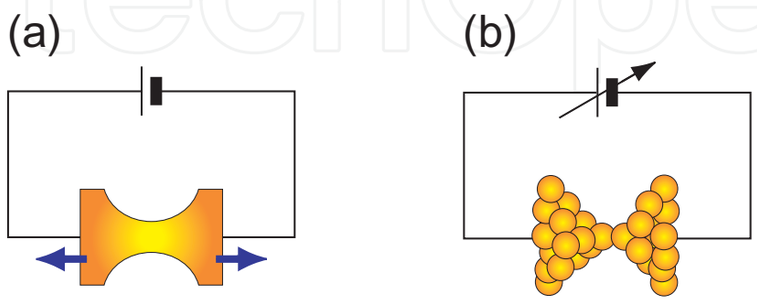

Fig. 5. Two methods for studying the high-bias instability of atom-sized contacts. In (a), a contact is mechanically stretched under high applied biases, whereas in (b), a single-atom contact is first produced and broken by applying a bias ramp.

In the method mentioned above, a contact usually fails before it shrinks to a single-atom. With this method, therefore, we are unable to study the instability of the single-atom contacts, and for studying single-atom contacts, another method shown in Fig. 5(b) is more suited. This method is basically an $I - V$ measurement of a contact but the upper bound of the bias is extended beyond the contact stability limit. First, a single-atom contact is fabricated under low biases. With maintaining the contact in its single-atom state, the bias is set to increase until the contact ruptures. The voltage and current at the contact failure determines the break voltage and current of the single-atom contact. Although this method sounds quite simple and easy to carry out, it is by no means a trivial matter to hold a single-atom contact for some time long enough for applying the bias ramp. Experiments are particularly difficult at room temperature where single-atom contacts are usually short-lived as suggested by Eq. 3. This method was first applied to the single-atom contacts of Au by Kim Hansen in his doctoral thesis, who named it the current disruption method. Then, the same method has been employed by Smit *et al.* (Smit et al., 2004) to determine the break voltage of Au and Pt single-atom contacts and chains at 4 K. All these previous measurements were performed at low temperatures to take an advantage of longer lifetime of single-atom contacts at cryogenic temperatures. In Sec. 5.2, we show our results on noble metals obtained at room temperature.

A noteworthy extension of this method is its application to molecular junctions where a single molecule is placed between a pair of nano-gapped electrodes. High-bias/current instability of various single-molecule junctions can also be investigated with the method shown in Fig. 5(b), provided that molecular bridges remain undestroyed until the onset of the high-bias instability. We carried out some experiments on junctions of thiol group molecules, and the results will be described in Sec. 5.4.

5.1 Current-induced instability

This section summarizes experimental results on the current-induced instability which happens in a metal nanocontact, the size of which is in nanometer scale but still larger than that of atoms. Experiments were carried out in ultrahigh vacuum at room temperature using the setup shown in Fig. 3.

As mentioned before, the current density in a contact increases with time when one breaks the contact by necking deformation under high biases. At some point in the course of contact necking, the contact becomes unstable and snipped off. This process can be monitored as shown in Fig. 6 where the time evolution of the conductance is depicted for Au, Ag, and Cu contacts under an applied bias of 2.0 V. Note that a conductance scale is quite nonlinear in the figure. Actually these plots are taken from oscilloscope traces, the vertical axis of which is not the conductance G but V_m in Eq. 7. As seen in Eq. 7, the conductance is a nonlinear function of V_m, and this nonlinearity between G and V_m largely distorts the vertical scale in Fig. 6, almost making it look like a logarithmic scale.

In all traces shown in Fig. 6, the conductance first decreases slowly and then becomes a bit accelerated. When the conductance reaches around several tens of G_0, it suddenly shows fluctuations and dives to zero. Because the vertical scale is nonlinear, the conductance fluctuations actually occur in large amplitudes. The onset of contact instability almost always accompanies such precursory conductance fluctuations. We first tried to characterize the instability by detecting the center of gravity of the conductance fluctuations, but some fluctuations are too short-lived to accurately determine the position of their gravity center. Alternatively, we detected the break conductance G_b, the last value of the conductance before

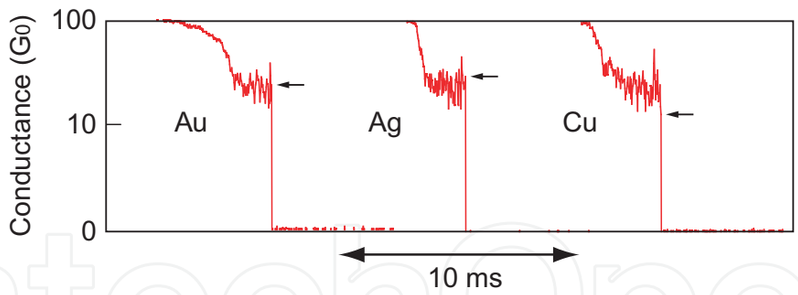

Fig. 6. Conductance traces of Au, Ag, and Cu contacts observed when they are stretched under an applied bias of 2.0 V. All contacts show significant conductance fluctuations before the contact failure. Arrows indicate the break conductance G_b, the last conductance value before the conductance jumps down. See text for the nonlinear conductance scale.

it jumps to zero. Each arrow in Fig. 6 indicates the break conductance of each contact. As seen in the figure, G_b is slightly off from the center of the fluctuations because, as seen in the case of Cu, the conductance sometimes jumps from the peak or the bottom of the fluctuation. Nevertheless, for many contacts, G_b serves as a reasonable parameter defining the onset of the instability.

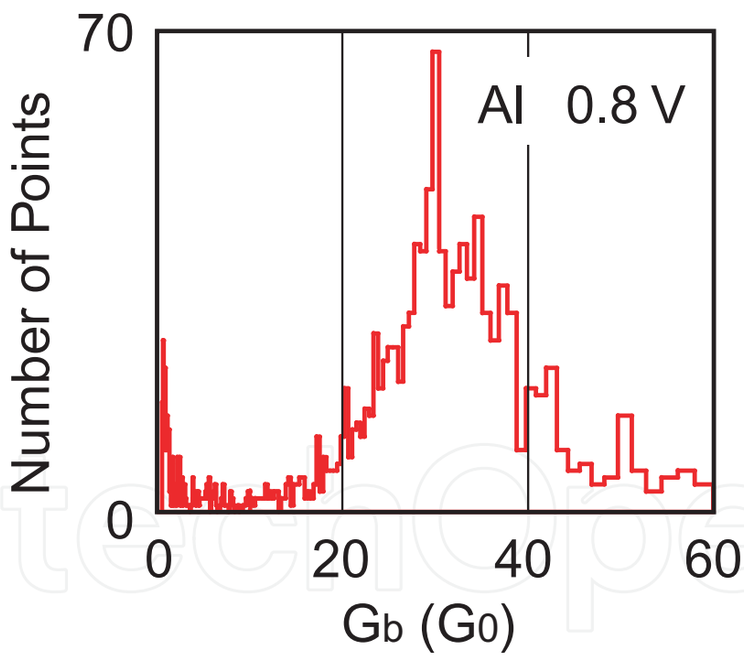

Fig. 7. Break conductance distribution for Al contacts obtained under an applied bias of 0.8 V.

We measured the break conductance for many contact breaks and constructed its histogram. An example of such break conductance histogram is shown in Fig. 7, this case for Al contacts at $V_a = 0.8$ V. The histogram exhibits a broad distribution with a single maximum, the position of which is denoted by $\hat{G}_b$. Similar broad and single-peak distribution is also observed for other metals when V_a is sufficiently high. A common feature of these break conductance histograms of various metals is that the peak position $\hat{G}_b$ changes with V_a and moves to the higher conductance side as V_a increases. Figure 8 shows a series of break conductance

histograms of Ag obtained under different V_a. Similar to that of Al shown in Fig. 7, the G_b distribution of Ag shows a single broad peak, the position of which is indicated by a stripe in each panel. Clearly, the peak position shifts to the higher conductance side as V_a increases. This means that a contact tends to break at a higher conductance under higher V_a.

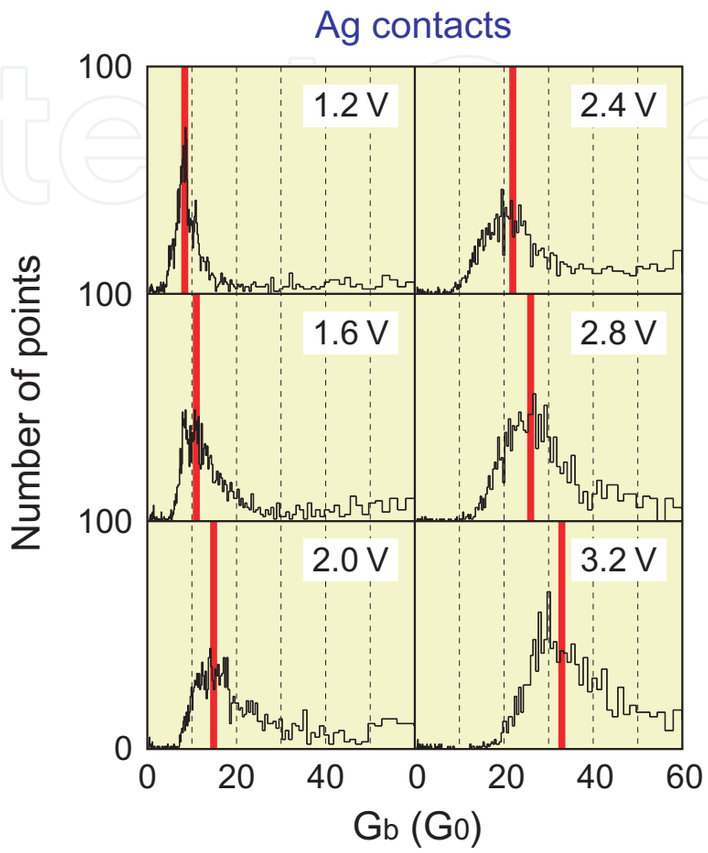

Fig. 8. Break conductance distribution for Ag contacts obtained under different applied biases. A strip marks the position of the distribution maximum, which shifts to the higher conductance side with increasing the applied bias.

To discuss this bias-induced shift of $\hat{G}_b$ more quantitatively, we made a plot shown in Fig. 9 where the contact current $\hat{I}_b$ corresponding to $\hat{G}_b$ is plotted against $\hat{G}_b$. As seen in the figure, the data points nicely fit to a straight line passing through the origin. This means $\hat{I}_b \propto \hat{G}_b$ or $\hat{I}_b/\hat{G}_b = (\text{const.})$. Figure 9 shows the example for Ag, but the same proportionality relationship between $\hat{I}_b$ and $\hat{G}_b$ can be found for noble metals, Au and Cu, and other metals such as Al (Minowa et al., 2005a), Zn (Suzuki et al., 2006), Pt (Minowa et al., 2005b), and Mo (Minowa et al., 2005b). The physical meaning of the observed proportionality between $\hat{I}_b$ and $\hat{G}_b$ can be understood if we notice that $\hat{G}_b$ is in the range of the Sharvin conductance and thus proportional to the contact area A as shown in Eq. 5. Then, $\hat{I}_b/\hat{G}_b = (\text{const.})$ can be rewritten as $\hat{I}_b/A = (\text{const.})$. Because $j_c \equiv \hat{I}_b/A$ is the contact current density, this result indicates that there is a current density, specific to each metal, at which a contact becomes unstable and breaks up.

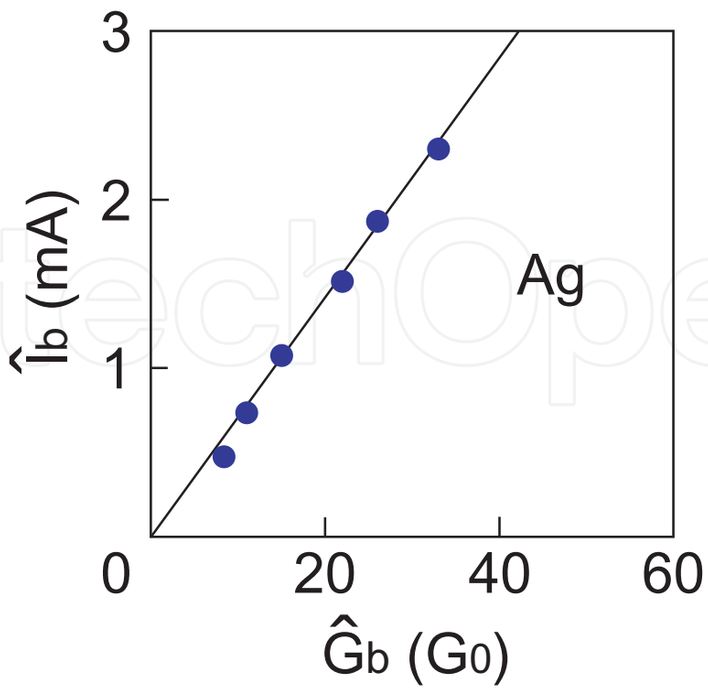

Fig. 9. $\hat{I}_b - \hat{G}_b$ plot for Ag contacts. The slope of the straight line determines the current density for the contact instability.

Figure 10 summarizes the experimental j_c of five metals estimated from the slope of the $\hat{I}_b - \hat{G}_b$ plot. In the figure, j_c is plotted against the melting temperature T_m of each metal. Though j_c of Au somehow deviates from others, a positive correlation is evident between j_c and T_m, i.e. metals of higher T_m show higher j_c. This result implies that the current-induced contact instability, and the marked conductance fluctuations shown in Fig. 6 as well, would be due to local contact melting. As seen in Fig. 10, the magnitude of j_c is in order of $10\mathrm{A/cm}^2$ which is three to four orders of magnitude higher than the current density flowing through interconnects in present-day microdevices. Significant Joule heating and local contact melting would thus be a plausible source of the observed contact failure. Another possibility is electromigration. Because the activation energy of electromigration empirically scales with T_m, electromigration can also account for the observed positive correlation between j_c and T_m. We, however, note that massive electromigration in atom-sized contacts would be effectively indistinguishable from local melting, and the distinction of two phenomena might be unnecessary. Whatever the instability mechanism is, the observed fast conductance fluctuations shown in Fig. 6 indicates that contact atoms would be quite mobile and nearly fluid-like at and near j_c.

A couple of remarks should be made on the magnitude and the meaning of j_c. First, j_c is estimated by applying the Sharvin conductance formula to the experimental $\hat{I}_b - \hat{G}_b$ relationship. Its magnitude of j_c, therefore, depends on the validity of the Sharvin conductance formula. Erts *et al.* (Erts et al., 2000) and Kizuka (Kizuka, 2008) carried out direct TEM observations of Au contacts simultaneously with the conductance measurements and showed that the Sharvin formula tends to underestimate the contact size. If A derived from Eq. 5 is smaller than the actual contact area, the true current density at the instability would

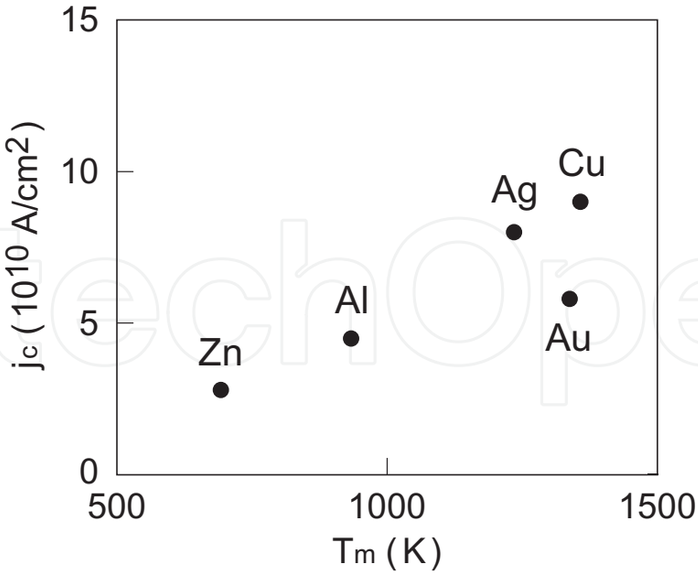

Fig. 10. Critical current density j_c for the contact instability is plotted against the melting point T_m of a metal. A linear correlation can be seen between j_c and T_m.

be lower than j_c shown in Fig. 10. For accurately determining j_c, we certainly need a reliable calibration formula that relates the conductance to the contact area. The Wexler conductance formula has been reported to yield better agreement with the TEM results than the Sharvin formula, but the Wexler formula contains a couple of fitting parameters, the values of which are unknown for most metals. Further accumulation of experimental data on the $G - A$ relationship of various metals is highly awaited for the accurate estimation of j_c.

Another parameter in the Sharvin formula that affects the magnitude of j_c is the Fermi wavevector k_F. As mentioned in Sec. 3, the Sharvin formula assumes a situation where free electrons pass through a small orifice. The formula is therefore applicable to the "nearly free-electron" metals such as Au and Al but not necessarily to transition metals whose d and f electrons cannot be treated as free electrons. This makes it difficult to estimate j_c of most transition metals. Pt contacts, for example, exhibit linear $\hat{I}_b - \hat{G}_b$ plot similar to that of noble metals. This result does not, however, yield j_c of Pt contacts because we cannot use the Sharvin formula for Pt to obtain the contact area. Again, the key issue is the lack of experimental $G - A$ data on various metals.

A contact breaks when its conductance becomes $\hat{G}_b$, and j_c is the current density at $G = \hat{G}_b$. In this context, j_c can be considered as the critical current density for the current-induced contact break. It should, however, be noted that $\hat{G}_b$ indicates the peak position of the break conductance distribution and represents the conductance at which a contact breaks with maximum likelihood. Because the distribution is not narrowly peaked at $\hat{G}_b$ but broadly extended as seen in Fig. 7, a substantial number of contacts break at conductances other than $\hat{G}_b$. Thus, j_c is a statistical quantity and should be understood as the current density at which a contact breaks with maximum likelihood. Not all contacts break at j_c with 100% probability. A considerable fraction of contacts would survive the instability and shrink to smaller contacts, some of them even becoming single-atom contacts. These highly stable contacts might be the source of single-atom contacts occasionally formed under very high biases close to 2 V.

Under such high biases, the current-induced instability at j_c acts as a selection filter which discriminates stable contacts from marginal ones.
As mentioned in Sec. 2, the stability or the lifetime of an atom-sized contact depends not only the bias but also the internal force F appearing in Eqs. 2 and 3. In the break junction method, one cannot control the details of contact necking when a contact shrinks to a nanocontact. Thus, the produced atom-sized contacts would have a built-in tensile force of different strengths, and this wide dispersion in F would be the source of varied contact stability and the broad distribution of G_b. The same situation happens for the break voltage as we will show in the next section.
When the applied bias becomes sufficiently low, the current-induced instability no longer happens during the contact necking, and majority of the contacts shrink down to the size of atoms. The break of such atom-sized contacts takes place at certain preferred contact geometries and the break conductance distribution shows a couple of narrow peaks found at some specific values corresponding to the conductance of these preferred geometries (Fujii et al., 2005). Different from the $\hat{G}_b$ peak, these peaks exhibit no shift with the bias. For $V_a < 1.0$ V, the break conductance of Au exhibits a sharp peak at $1G_0$ showing that most Au contacts break after they shrink to the single-atom contact. On the other hand, the same single-atom break becomes abundantly observed for Ag and Cu only at $V_a < 0.1$ V and $V_a < 0.3$ V, respectively. This comparison clearly indicates the superior high-bias stability of the single-atom contact of Au, which will be further discussed in the next section.

5.2 Break voltage

Under high applied biases, only the contacts of higher stability can survive the current-induced instability and become the single-atom contact. Experimental results on such instability-selected contacts would provide us biased information on the contact stability and cannot represent the high-bias/current stability of a majority of the single-atom contacts. To obtain proper information, it is therefore necessary to first produce single-atom contacts under low biases and then examine their stability by increasing the bias voltage and detecting the breakdown threshold. This is the experimental method depicted in Fig. 5(b).
As mentioned before, the first break-voltage measurement on a single-atom contact has been made by Hansen who used an Au-tip/Au-sample STM junction and produced the single-atom contacts of Au at 77 K in ultrahigh vacuum. By applying a fast voltage ramp, he could observe the contact disruption and measured the bias at the contact failure. He obtained the integral distribution of the break voltage and found that 90% of the Au single-atom contacts break at ~ 1.9 V. Subsequently, Smit and coworkers (Smit et al., 2004) carried out a systematic study of the break voltage of Au and Pt single-atom contacts exploiting cryogenic MCBJ operated at 4 K, where atomic contacts and chains are stable almost indefinitely. Smit *et al.* could investigate not only the break voltage distribution but also its dependence on the atomic chain length. For the shortest single-atom chain, the break voltage distribution yields a mean break voltage ~ 1.2 V and ~ 0.37 V for Au and Pt, respectively.
Though these previous results obtained at low temperatures provide us a good measure of the break voltage of metal single-atom contacts, similar break-voltage experiments at room temperature are also needed for two reasons. First, for practical device applications, break voltage data at room temperature are more valuable, for example, for establishing the maximum rating of the single-atom contacts as device interconnects. Second, at room temperature, there would be less ambiguity in the contact temperature than at cryogenic

temperatures. As noted in Sec. 2, contacts can be significantly heated up at high biases when the ambient temperature is lower than the characteristic temperature T_V in Eq. 4. In experiments at 4 K, for example, the effective contact temperature at the break voltage of 1.2 V should not be 4 K but $\sim$ 46 K. On the other hand, at room temperature, the ambient temperature overwhelms T_V in Eq. 4, and the contact heating becomes negligible at 1.2 V. In return for these advantages, the single-atom contacts become short-lived at room temperature, and we have to carry out fast measurements for determining their break voltage.

Our procedures for measuring the break voltage of single-atom contacts are the following (Miura et al., 2009). First, a constant bias of 0.1 V is applied across a $(\text{contact}) + R$ where R is a current-sensing resistor. When the contact is made open, the contact current decreases with reducing the contact size and reaches to a value corresponding to the single-atom conductance, which is $1G_0$ for noble metals. If the single-atom state is stable for some time, the current remains constant and exhibits a plateau. Upon detecting such a $1G_0$ current plateau, the bias is set to increase and the current increases accordingly. At a certain point, the contact ruptures and the current jumps down to zero. The break voltage can be obtained from the maximum applied bias before the contact failure. Figure 11 shows (a) the experimental setup and (b) a typical result of the break voltage measurement made, in this case, on an Au contact. Fabrication of single-atom contacts is made with the MCBJ method which has been briefly explained in Sec. 4. In Fig. 11(a), a block diagram of the conductance measuring circuit is also included. As in the experiment on the current-induced instability, a fast oscilloscope is used to monitor conductance transients at and near the contact breakdown. The conductance or the current can be obtained by measuring the voltage drop across R. The measured contact current is shown in the upper panel in Fig. 11(b). It decreases with time and, at point A in the figure, exhibits a plateau. This plateau appears at the current level corresponding to $1G_0$ and hence signifies the formation of an Au single-atom contact. A trigger signal is generated at point A to start the bias ramp but delayed through a delay circuit before activating the bias source as shown in Fig. 11(a). As a result of this delay, the bias actually starts to increase at point B in the lower panel. The delay time is 40μs for Au and Cu and 10μs for Ag, Al, and AuAg alloys. This delay is needed to screen out marginal single-atom contacts. Upon starting the bias ramp, the contact current in the upper panel Fig. 11(b) increases linearly with time and suddenly drops to zero at point C which marks the contact breakdown. At a closer look, the contact current falls down not instantaneously but within a non-zero time interval, making it difficult to sharply define the point of breakdown. We therefore arbitrarily defined the breakdown point by the maximum of the $I(t)$ curve. By taking into account the correction for the voltage drop across R, the break voltage is calculated as $V_b = V_a - IR$ where V_a and I are their values at the current maximum.

Figure 12 summarizes the break voltage distribution measured for four metals at room temperature in ultrahigh vacuum. As for the break conductance shown in Figs. 7 and 8, a broad and single-peak distribution is commonly observed for the break voltage of four metals. The distribution of Cu appears relatively narrower, but its peak still covers a wide voltage range from 0.2 V to 1.4 V. In the case of Au, the break voltage distribution extends beyond 2 V. This is not the thermal broadening because a similar broad distribution is also observed for the break voltage of Au single-atom contacts at cryogenic temperatures. In Sec. 5.1, we pointed out that the wide distribution of the break conductance would be due to large fluctuations in the strength of the built-in tensile force F in Eqs. 2 and 3. The same fluctuations in F would also be responsible for the broadening of the break voltage distribution.

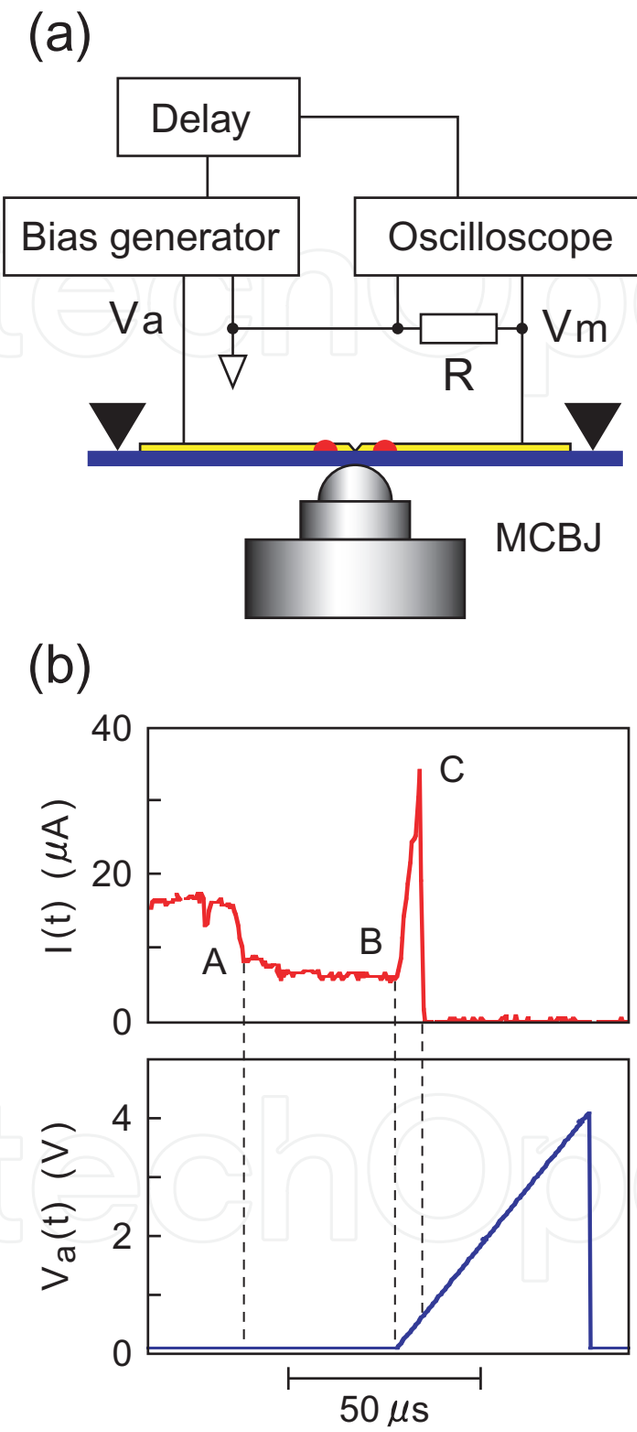

Fig. 11. Experimental setup (a) and typical temporal changes in the contact current and the bias voltage (b) in the break voltage measurements on an Au single-atom contact. See text for details.

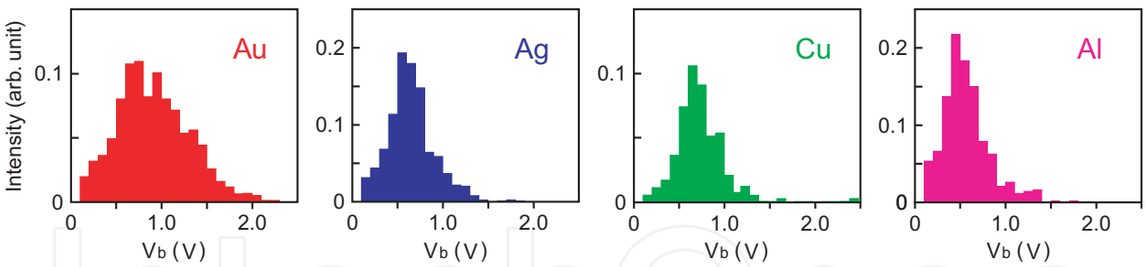

Fig. 12. Break voltage distribution obtained on single-atom contacts of Au, Ag, Cu, and Al at room temperature in ultrahigh vacuum.

The average break voltage is $V_b(\mathrm{Au}) = 0.93$ V. $V_b(\mathrm{Ag}) = 0.65$ V. $V_b(\mathrm{Cu}) = 0.69$ V. and $V_b(\mathrm{Al}) = 0.58$ V for Au, Ag, Cu, and Al single-atom contacts, respectively. This comparison simply indicates the superior high-bias stability of Au single-atom contacts over those of other metals. As we mentioned at the end of the previous section, the same conclusion is indirectly suggested from the break conductance data. The results of the break voltage experiment shown in Fig. 12 directly and quantitatively prove the high stability of the Au single-atom contact against high biases.

If we assume that the contact break occurs when $E(V,F) \sim k_BT$ in Eq. 3, then $V_b = (E_0 - \beta F - k_BT^*)/\alpha$ as we mentioned in Sec. 2. Thus, the observed higher V_b indicates larger E_0 for the Au single-atom contact than that for Ag and Cu contacts, provided that βF would be the same for all metals. As mentioned in Sec. 2, Smit *et al.* (Smit et al., 2004) report $E_0(\mathrm{Au}) = 0.738$ eV. No data are, however, available for E_0 of other metals so that we cannot know whether $E_0(\mathrm{Au})$ is actually the largest or not. Some clues can, however, be obtained from the break force, i.e. the maximum tensile strength, of single-atom contacts. As for the break voltage, the break force can be expressed as $F_b = (E_0 - \alpha V - k_BT^*)/\beta$, and a larger E_0 would yield a higher F_b. Again, the experimental value of F_b has been obtained only for two metals, Au and Pt, which show $F_b(\mathrm{Au}) \sim 1.5$ nN (Rubio-Bollinger et al., 2001), and $F_b(\mathrm{Pt}) \sim 1$ nN (Kizuka & Monna, 2009), respectively. Fortunately, however, theoretical values are available for F_b of other metals (Bahn & Jacobsen, 2001; Pauly et al., 2006). Though the magnitude of the calculated F_b does not necessarily conform well to the experimental values, all theories consistently predict higher tensile strength of Au and Pt single-atom contacts than that of Ag, Cu, and Ni. Thus, the observed higher $V_b(\mathrm{Au})$ is consistent with the results of these break force studies. It should, however, be noted that the estimation of V_b from E_0 or F_b depends on the value of α and β in Eq. 3, and the comparison of E_0 and F_b of different metals would be meaningful only when these parameters little depend on metal species. As mentioned in Sec. 2, measurements of the conductance TLFs indicate that noble metals show nearly the same α (Tsutsui et al., 2006b). It thus seems not unreasonable to assume little variation of α and β among metals, and the higher F_b of the Au single-atom contacts would be correlated with our observation of their higher V_b.

5.3 Break voltage of alloy contacts

In bulk alloys, foreign solute atoms usually act as a scattering center of electrons. Alloying, therefore, decreases the conductivity of host metals. This is, however, not the case of alloy single-atom contacts. The single-atom conductance of Au and Cu, for example, shows no substantial changes with the addition of Pd and Ni, respectively, up to a concentration as

high as 50 at% (Bakker et al., 2002; Enomoto et al., 2002). In the conductance histogram of AuPd and CuNi alloys, the single-atom peak of Au and Cu remains at $1G_0$ and stays unshifted with alloying, though its intensity decreases nearly linearly with increasing the solute concentration. This result indicates that the single-atom conductance of alloy contacts is locally determined by the elemental species of an atom occupying the contact site. When a single Cu atom comes to the linking site, for example, the conductance becomes the single-atom conductance of Cu ($G = 1G_0$), while it changes to that of Ni ($\sim 1.3G_0$) when a Ni atom replaces the Cu atom. Such a conductance switching associated with the replacement of the contact atom has been actually observed on AuPt alloys (Heemskerk et al., 2002). Other alloy atoms locating nearby the contact site only make secondary contributions to the single-atom conductance.

Similar locality can thus be naturally expected for the break voltage of alloy single-atom contacts. Figure 13 shows the break voltage distribution obtained on the single-atom contacts of an Au-31at

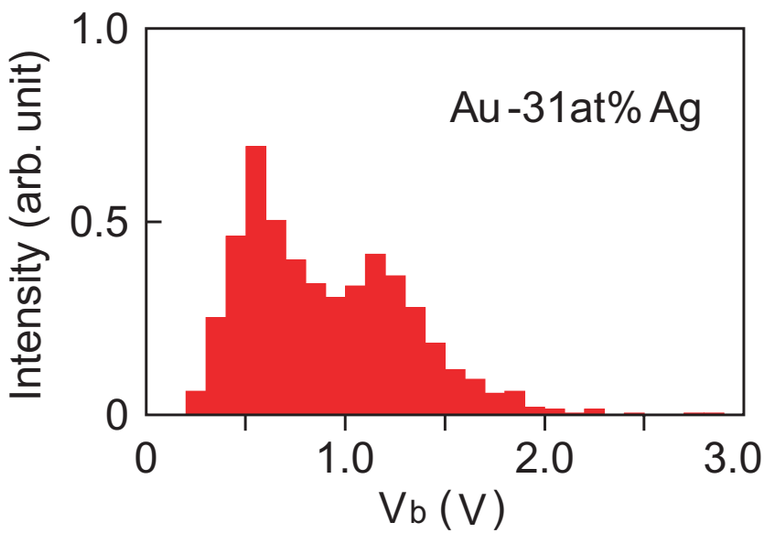

Fig. 13. Break voltage distribution obtained on single-atom contacts of an Au-31at%Ag alloy.

5.4 Molecular junctions

Break-voltage measurements can be extended to single-molecule junctions or molecular links, where a single molecule, instead of a metal atom, bridges a pair of metal electrodes. Molecules in such junctions can be of full variety in species and in configurations and able to show various functionalities unobtainable by single metal atoms. As a result, single-molecule junctions are considered as a key active element in molecular devices, and a soaring number of theoretical and experimental studies have been made on various single-molecule junctions in the past decade.

Most of the previous studies are, however, concerned with the low-bias regime where the junction conduction is determined by the transmission function near the electrode Fermi level. However, many molecules have their HOMO and LUMO levels which do not necessarily locate near the Fermi level. As a result, the conduction through molecular junctions is usually made through the tail states of the HOMO and LUMO levels which are broadened by the

molecule-electrode coupling. To take various benefits of the resonant conduction through the HOMO and LUMO levels, one therefore has to apply high biases to encompass the HOMO and LUMO levels into the bias window. There is, however, no information as to how high biases one can apply to a single-molecule junction before it breaks down. A large number of $I-V$ measurements have been made on various single-molecule junctions, and a few of them report the existence of a bias threshold beyond which a junction becomes unstable. However, such a high-bias threshold has been rarely studied in previous experimental investigations.

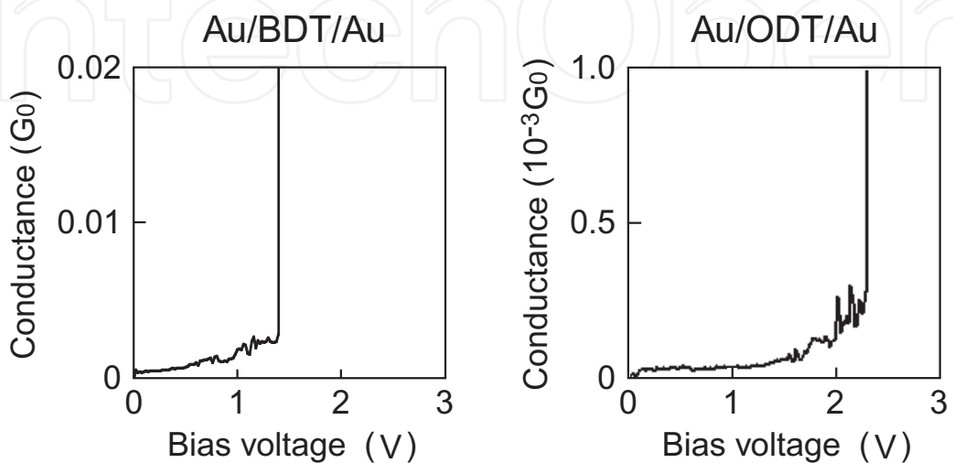

Fig. 14. High-bias instability observed on Au/BDT/Au and Au/ODT/Au single-molecule junctions at room temperature. The conductance jumps up at the instability.

Figure 14 shows a typical behavior of the molecular conductance when the bias surpasses the threshold (Hashimoto et al., unpublished; Teramae et al., 2008). Two conductance-voltage curves are shown for Au/benzenedithiol (BDT)/Au and Au/octanedithiol (ODT)/Au single-molecule junctions measured in Ar atmosphere at room temperature. The low-bias conductance of these junctions is $0.01G_0$ and $5 \times 10^{-4}G_0$, respectively. In both $G-V$ curves, the conductance first increases slowly with the bias and indicates positive nonlinearity in the $I-V$ characteristics. At a threshold, the conductance jumps up, showing that the junction is coalesced. This high-conductance state remains until the junction is made open by mechanically pulling apart the electrodes.

The distribution of the threshold voltage V_{th} is shown in Fig. 15 (Hashimoto et al., unpublished; **?**). For both Au/BDT/Au and Au/ODT/Au junctions, the distribution is broad and single-peaked, quite similar to the break-voltage distribution of single-atom contacts of metals shown in Fig. 12. It is also noted in the figure that the less conductive Au/ODT/Au junction shows higher threshold voltage compared to that of the Au/BDT/Au junctions.

This dependence of the threshold voltage on the (low-bias) junction conductance can be seen more clearly in Fig. 16 where the average threshold is plotted against the logarithm of the junction resistance $\log R$. Both Au/BDT/Au and Au/ODT/Au junctions are known to take a couple of junction states of different conductances, and the threshold data of these different states (three for Au/BDT/Au and two for Au/ODT/Au, respectively) are included in the plot. The resistances of Au/BDT/Au and Au/ODT/Au junctions differ by two orders of magnitude, but their threshold data lay on a single straight line.

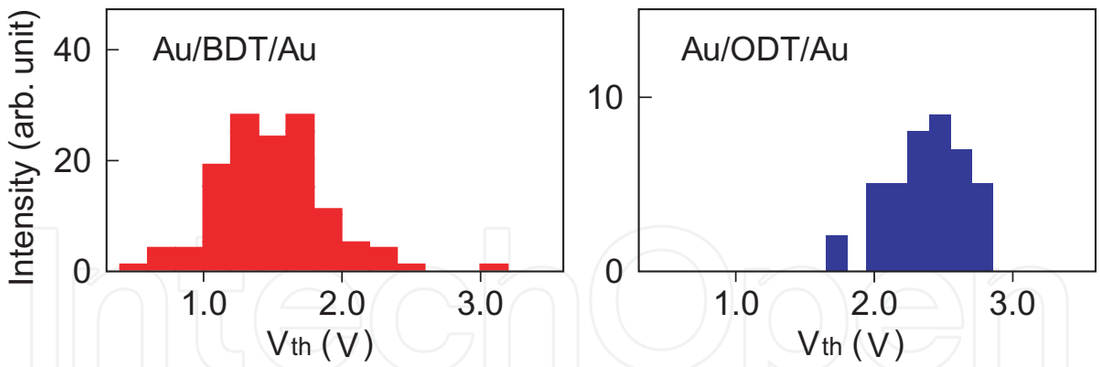

Fig. 15. Distribution of the instability threshold voltage obtained on Au/BDT/Au and Au/ODT/Au single-molecule junctions.

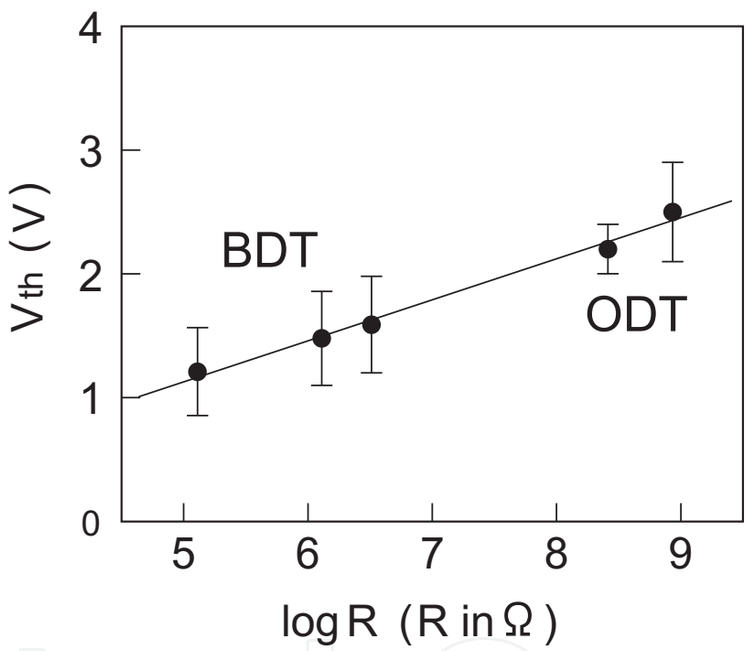

Fig. 16. Dependence the instability threshold on log R.

As log R of molecular junctions scales roughly linearly with the molecular length, or the electrode separation of the junction, the observed linear correlation between V_{th} and log R indicates the existence of a critical field strength for the onset of the junction instability. Also, the observation that the V_{th} data of different molecular junctions lay on the same straight line indicates that a crucial parameter for the instability is not the species of bridging molecule but the magnitude of log R or the electrode gap distance. This means that in the high-bias instability of single-molecule junctions, the molecule merely acts as an insulating material separating electrodes and defining its gap distance. Chemical properties of the bridging molecule little matter for the instability threshold. It should be noted that similar field-induced coalescence of electrodes is also observed in the high-bias breakdown of STM tunnel junctions (Mamin et al., 19908) and Au/alkane-SAM/Au junctions (Wold & Frisbie, 2001; Zhao & Uosaki, 2001).

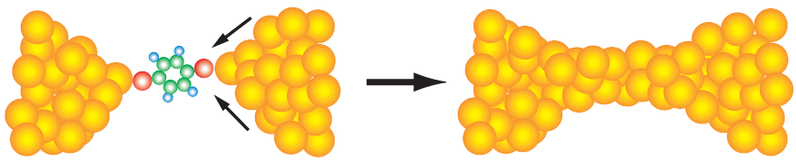

Fig. 17. Possible breakdown or collapse of electrodes at the high bias instability.

Because the junction conductance jumps up at the threshold as shown in Fig. 14, the electrodes are likely to become coalesced when the bias reaches the threshold, as schematically illustrated in Fig. 17. In such a case, the high-bias instability takes place not inside the molecule but at the electrodes. Thus, for improving the toughness of molecular junctions against high biases, one has to first select electrode materials more resistant to the high-bias collapse than Au.

5.5 Concluding remark

With recent developments in experimental techniques such as SPM and MCBJ, we can now routinely fabricate single-atom or single-molecule junctions, which are the smallest functional contact realizable in the world. We have already accumulated a large amount of knowledge on the conductance or the resistance of these ultrasmall junctions, and the mechanisms of their electronic conduction have been well documented. Still, we cannot answer a simple question how large electronic current one can flow through these junctions. Considering a huge number of studies devoted to atomic and molecular junctions, it seems quite strange that so few studies have been made on this academically interesting and practically important problem. Our experimental results described in this article have clarified some aspects of the high-bias/current instability for atom-sized contacts of a few metals and molecules, but there remain a large number of atomic scale junctions, the stability of which has been yet unexplored and awaits further experimental investigations. One noticeable characteristic, common to all three parameters G_b, V_b and V_{th} studied in this work, is the appreciable broadening of their distribution. As we mentioned before, this broadening is likely due to fluctuations in the strength of the internal tensile force F acting on the breaking contacts. To make the distribution narrower and improve the accuracy of instability parameters, it would therefore be necessary to control the strength of F in each contact. High-bias experiments on such force-controlled contacts would provide us a direct test of Eq. 3 and give some useful insight about the microscopic origin of that empirical equation.

Acknowledgements

The author would like to thank his former graduate students T. Minowa, A. Fujii, M. Tsutsui, Y. Teramae, and D. Miura for their carrying out various high-bias experiments described in this article. This work is partially supported by KAKENHI 17310072.

6. References

Agraït, N.; Levy Yeyati, A. & and van Ruitenbeek, J. M. (2003). Quantum properties of atomic-sized conductors. *Physics Reports* 377, 81-279.

Bahn S. R. & Jacobsen, K. W. (2001). Chain formation of metal atoms *Physical Review Letters* 87, 266101(1-4).

Bakker, D. J.; Noat, Y.; Yanson, A. I. & van Ruitenbeek, J. M. (2002). Effect of disorder on the conductance of a Cu atomic point contact. *Physical Review B* 65, 235416(1-5).

Cuevas, J. C.; Levy Yeyati, A. & Martín-Rodero, A. (1998). Microscopic origin of conductance channels in atomic-size contacts. *Physical Review Letters* 80, 1066-1069.

Enomoto, A.; Kurokawa, S. & Sakai, A. (2002). Quantized conductance in Au-Pd and Au-Ag alloy nanocontacts. *Physical Review B* 65, 125410(1-6).

Erts, D.; Olin, D.; Ryen, L.; Olsson, E. & Tholen, A. (2000). Maxwell and Sharvin conductance in gold point contacts investigated using TEM-STM. *Physical Review B* 61, 12725(1-3).

Fujii, A.; Tsutsui, M.; Kurokawa, S. & Sakai, A. (2005). Break conductance of noble metal contacts. *Physical Review B* 72, 045407(1-6).

Hashimoto, S.; Kurokawa, S. & Sakai, A. *unpublished*.

Heemskerk, J. W. T.; Noat, Y.; Bakker, D. J.; van Ruitenbeek, J. M.; Thijsse, B. J. & Klaver, P. (2003). Current-induced transition in atomic-sized contacts of metallic alloys. *Physical Review B* 67, 115416(1-5).

Kizuka, T. (2008). Atomic configuration and mechanical and electrical properties of stable gold wires of single-atom width. *Physical Review B* 77, 155401(1-11).

Kizuka T. & Monna K. (2009). Atomic configuration, conductance, and tensile force of platinum wires of single-atom width. *Physical Review B* 80, 205406(1-9).

Mamin, H. J.; Guethner, P. H. & Rugar, D. (1990). Atomic emission from a gold scanning-tunneling-miscroscope tip. *Physical Review Letters* 65, 2418-2421.

Minowa, T.; Kurokawa, S. & Sakai, A. (2005). Break Conductance of Al Nanocontacts. *Physica E* 29, 495-499

Minowa, T.; Tsutsui, M.: Kurokawa, S. & Sakai, A. (2005). Break conductance of Pt nanocontacts. *Japanese Journal of Applied Physics* 44, 6321-6326.

Miura, D.; Iwata, K.; Kurokawa, S. & Sakai, A. (2009). Break voltage of the $1G_0$ contact of noble metals and alloys. *e-Journal of Surface Science and Nanotechnology* 7, 891-897.

Pauly, F.; Dreher, M.; Viljas, J. K.; Häfner, M.; Cuevas, J. C. & Nielaba, P. (2006). Theoretical analysis of the conductance histograms and structural properties of Ag, Pt, and Ni nanocontacts. *Physical Review B* 74, 235106(1-21).

Rubio-Bollinger, G.; Bahn, S. R.; Agraït, N.; Jacobsen, K. W. & Vieira, S. (2001). Mechanical properties and formation mechanisms of a wire of single gold atoms. *Physical Review Letters* 87, 026101(1-4).

Smit, R. H. M.; Untiedt, C. & Ruitenbeek, J. M. (2004). The high-bias stability of monoatomic chains. *Nanotechnology* 15, S472-S478.

Suzuki, R.; Mukai, Y.; Tsutsui, M.: Kurokawa, S. & Sakai, A. (2006). Conductance of atom-sized Zn contacts. *Japanese Journal of Applied Physics* 45, 7217-7223.

Teramae, Y.; Horiguchi, K.; Hashimoto, S.; Tsutsui, M.: Kurokawa, S. & Sakai, A. (2008). High-bias breakdown of Au/1,4benzenedithiol/Au junctions. *Applied Physics Letters* 93, 083121(1-3).

Todorov, T. N.; Hoekstra, J. & Sutton, A. P. (2001). Current-induced embrittlement of atomic wires. *Physical Review Letters* 86, 3606-3609.

Tsutsui, M.; Kurokawa, S. & Sakai, A. (2006). Bias-induced local heating in Au atom-sized contacts. *Nanotechnology* 17, 5334-5338.

Tsutsui, M.; Shoji, K,; Taniguchi, M. & and Kawai, T. (2008). Formation and self-breaking mechanism of stable atom-sized junctions. *Nano Letters* 8, 345-349.

Tsutsui, M.; Teramae, Y.; Kurokawa, S. & Sakai, A. (2006). Local heating in noble metal nanocontacts under high biases at 77 K. *Applied Surface Science* 252, 8677-8682.

Wold D. J. & Frisbie, C. D. (2001). Fabrication and characterization of metal-molecule-metal junctions by conducting probe atomic force microscopy. *Journal of American Chemical Society* 123, 5549-5556.

Yanson, A. I.; Rubio-Bollinger, G.; van den Brom, H. E.; Agraït, N. & van Ruitenbeek, J. M. (1998). Formation and manipulation of a metallic wire of single gold atoms. *Nature (London)* 395, 783-785.

Zhao, J. & Uosaki, K. (2003) Dielectric properties of organic monolayers directly bonded on silicon probed by current sensing atomic force microscope. *Applied Physics Letters* 83, 2034-2036.

Nanowires - Fundamental Research

Edited by Dr. Abbass Hashim

ISBN 978-953-307-327-9
Hard cover, 552 pages
Publisher InTech
Published online 19, July, 2011
Published in print edition July, 2011

Understanding and building up the foundation of nanowire concept is a high requirement and a bridge to new technologies. Any attempt in such direction is considered as one step forward in the challenge of advanced nanotechnology. In the last few years, InTech scientific publisher has been taking the initiative of helping worldwide scientists to share and improve the methods and the nanowire technology. This book is one of InTechâ€™s attempts to contribute to the promotion of this technology.

How to reference

In order to correctly reference this scholarly work, feel free to copy and paste the following:

Akira Sakai (2011). High-Bias Instability of Atomic and Molecular Junctions, Nanowires - Fundamental Research, Dr. Abbass Hashim (Ed.), ISBN: 978-953-307-327-9, InTech, Available from: http://www.intechopen.com/books/nanowires-fundamental-research/high-bias-instability-of-atomic-and-molecular-junctions

INTECH
open science | open minds

InTech Europe
University Campus STeP Ri
Slavka Krautzeka 83/A
51000 Rijeka, Croatia
Phone: +385 (51) 770 447
Fax: +385 (51) 686 166
www.intechopen.com

InTech China
Unit 405, Office Block, Hotel Equatorial Shanghai
No.65, Yan An Road (West), Shanghai, 200040, China
中国上海市延安西路65号上海国际贵都大饭店办公楼405单元
Phone: +86-21-62489820
Fax: +86-21-62489821

IntechOpen